

Jasna Ivanovic, Kurosch Rezwan, Stephen Kroll

Supercritical CO₂ deposition and foaming process for fabrication of biopolyester-ZnO bone scaffolds

Journal Article as: peer-reviewed accepted version (Postprint)

DOI of this document* (secondary publication): 10.26092/elib/2627

Publication date of this document: 10/11/2023

* for better findability or for reliable citation

Recommended Citation (primary publication/Version of Record) incl. DOI:

Ivanovic, J., Rezwan, K. and Kroll, S. (2017),
Supercritical CO₂ deposition and foaming process for fabrication of biopolyester-ZnO bone scaffolds.
J. Appl. Polym. Sci., 135, 45824,
doi: 10.1002/app.45824

Please note that the version of this document may differ from the final published version (Version of Record/primary publication) in terms of copy-editing, pagination, publication date and DOI. Please cite the version that you actually used. Before citing, you are also advised to check the publisher's website for any subsequent corrections or retractions (see also <https://retractionwatch.com/>).

"This is the peer reviewed version of the following article: Ivanovic, J., Rezwan, K. and Kroll, S. (2017), Supercritical CO₂ deposition and foaming process for fabrication of biopolyester-ZnO bone scaffolds. J. Appl. Polym. Sci., 135, 45824, doi: 10.1002/app.45824, which has been published in final form at <https://doi.org/10.1002/app.45824>. This article may be used for non-commercial purposes in accordance with Wiley Terms and Conditions for Use of Self-Archived Versions. This article may not be enhanced, enriched or otherwise transformed into a derivative work, without express permission from Wiley or by statutory rights under applicable legislation. Copyright notices must not be removed, obscured or modified. The article must be linked to Wiley's version of record on Wiley Online Library and any embedding, framing or otherwise making available the article or pages thereof by third parties from platforms, services and websites other than Wiley Online Library must be prohibited."

This document is made available with all rights reserved.

Take down policy

If you believe that this document or any material on this site infringes copyright, please contact publizieren@suub.uni-bremen.de with full details and we will remove access to the material.

Supercritical CO₂ deposition and foaming process for fabrication of biopolyester–ZnO bone scaffolds

Jasna Ivanovic ¹, Kurosch Rezwan,^{2,3} Stephen Kroll^{2,3}

¹Faculty of Technology and Metallurgy, Department of Organic Chemical Technology, University of Belgrade, Karnegijeva 4, Belgrade 11000, Republic of Serbia

²Advanced Ceramics, University of Bremen, Am Biologischen Garten 2, Bremen 28359, Germany

³Centre for Materials and Processes (MAPEX), University of Bremen, Bibliothekstraße 1, Bremen 28359, Germany
Correspondence to: J. Ivanovic (E-mail: jasnai@tmf.bg.ac.rs)

ABSTRACT: Subsequent supercritical CO₂-assisted deposition and foaming process followed by *in situ* synthesis was used to fabricate functional polylactide (PLA) and polylactide–poly(ϵ -caprolactone) (PLA–PCL) bone scaffolds. Deposition of zinc bis(2-thenoyltri-fluoroacetate) as a ZnO precursor onto biopolyester substrates (30 MPa; 110 °C) was followed by fast depressurization to create cellular structure. Contact time was optimized regarding the deposition yield (2 h), while PCL content in PLA was varied (1–10 wt %). Scaffolds impregnated with the precursor were treated with hydrazine alcoholic solution to obtain biopolyester–ZnO composites. Precursor synthesis and deposition onto the scaffolds was confirmed by Fourier-transform infrared. Processed scaffolds had micron-sized pores ($d_{50} \sim 20 \mu\text{m}$). High open porosity (69–77%) and compressive strength values (2.8–8.3 MPa) corresponded to those reported for trabecular bone. PLA blending with PCL positively affected precursor deposition, crystallization rate, and compressive strength of the scaffolds. It also improved PLA surface roughness and wettability which are relevant for cell adhesion. ZnO improved compressive strength of the PLA scaffolds without significant effect on thermal stability. Analysis of structural, thermal, and mechanical properties of biopolyester–ZnO scaffolds testified a great potential of the obtained platforms as bone scaffolds. Proposed processing route is straightforward and ecofriendly, fast, easy to control, and suitable for processing of thermosensitive polymers. © 2017 Wiley Periodicals, Inc. *J. Appl. Polym. Sci.* **2018**, *135*, 45824.

KEYWORDS: biomedical applications; biopolymers and renewable polymers; composites; foams; manufacturing

INTRODUCTION

Composites of bioresorbable polymers containing inorganic fillers have been extensively investigated for fabrication of porous nanostructured materials for bone tissue engineering (BTE) applications.^{1,2} Saturated biodegradable and biocompatible poly(α -hydroxy esters), including poly(lactic acid) (PLA), poly(ϵ -caprolactone) (PCL), poly(glycolic acid) (PGA), and poly(lactic acid-co-glycolic acid) (PLGA) are the most often utilized synthetic biopolymers for three-dimensional scaffolds in tissue engineering.³ PLA is particularly attractive due to its sustainable production, good processability and mechanical properties.⁴ It is approved by Food and Drug Administration (FDA) and has already demonstrated proof-of-concept for a wide range of biomedical applications, including biodegradable sutures, bone fixation, soft-tissue implants, drug delivery devices, tissue engineering, and craniofacial augmentations in plastic surgery.^{5,6} PLA has been also considered

for fabrication of porous three-dimensional scaffolds^{5,7} and membranes^{8–12} for bone tissue regeneration.

The main shortcomings of PLA are low ductility and toughness, slow crystallization, poor thermal resistance, sensitivity to moisture and thereby degradation by hydrolysis.¹³ Poly(ϵ -caprolactone) as a biodegradable aliphatic polyester has lower tensile strength, slower degradation rate and better toughness than PLA.¹⁴ There is a large difference in bulk properties of PLA with PCL.¹⁴ Therefore, their blends and copolymers were suggested for creation of new biomaterials with tailored mechanical, thermal, and viscoelastic and biodegradation properties suitable for the given environmental or physiological conditions.^{14–17}

Commonly methods used to generate highly porous PLA-based polymer or composite materials for tissue engineering such as solvent casting/salt leaching,^{18,19} fiber forming²⁰ and 3D printing²¹ require use of liquid solvents and/or a drying step (i.e.,

freeze drying). Introduction of thermal gradients during drying (i.e., freeze drying process) can result in undesirable anisotropy of pore size and alignment. Melt blending or extrusion is favorable for fabrication of PLA-based composites because of its versatility and environmental friendliness since no solvents are used. The optimization of this process is, however, challenging regarding nanolevel dispersion of particles and ensuring structural integrity of the nanofillers.²² Apart from that, the processing method and temperature regime should have minimal adverse effects on the PLA matrix which is prone to degradation above 180 °C.²³

The solid-state foaming using supercritical carbon dioxide (scCO₂) has been extensively studied for controlled and environmentally friendly production of nano- and microcellular polymeric foams^{24–26} with particular focus on biodegradable platforms for tissue engineering and drug delivery devices.^{2,27} It involves CO₂ dissolution in amorphous fraction of polymer matrix followed by inducing of thermodynamic instability (i.e., a pressure quench) that causes phase separation. Supersaturation of the blowing agent results in the nucleation of gas bubbles and a cellular structure grows as dissolved gas escapes from the polymer/gas mixture.^{24,28} Setting the target viscosity of the polymer/gas solution and locking-in the desirable phase morphologies (pore size and crystallinity) as cells develop during the phase separation are essential for generation, growth and connectivity of pores.²⁸ Polymer conversion to foam structures usually leads to a loss in the mechanical strength due to the presence of gas bubbles inside.²⁷

Therefore, nano- and micron-sized inorganic fillers (i.e., clays, apatite, talc, and carbon) are used to improve mechanical and bioactive properties of the polymeric scaffolds.^{2,18,29–31} Some metals (Ti, Ag, Zn, Cu, Mg, Ca, Ce, Yt, and Al) and their oxides have proven antimicrobial activity.³² Beside strong antimicrobial activity,³³ ZnO was reported for its significant roles in bone health and formation.^{34,35} Zinc oxide–nanoparticles (ZnO–NPs) have been recently considered as a coating material for orthopedic and dental implants used to inhibit bacterial adhesion and promote osteoblast growth.³⁶ Immobilization of ZnO–NPs into poly(DL-lactide-co-glycolide) polymer matrix has been recently reported as promising drug delivery system for prevention and elimination of bacterial and fungal infections at minimal inhibitory concentrations of 0.5–0.6 mg/mL and without cytotoxic response.³⁷

Supercritical fluid deposition (SCFD) using scCO₂ has recently emerged as an attractive alternative process for controlled dispersion of metallic species atomically or as nanoparticles onto internal surface of solid substrates at relatively low temperatures.³⁷ It involves metal complex (precursor) dissolution in a supercritical fluid (SCF) and its adsorption onto support structures followed by the conversion of the adsorbed complex to the target metal species. Dissolution of dense CO₂ in polymers increases chain mobility which thereby acts like molecular lubricant and causes polymer swelling.^{39–42} This enables processing of polymer at lower temperatures^{26,43,44} and facilitates incorporation of compounds soluble in SCF.⁴⁵ The metallic precursor is reduced to the desired metal form

by chemical reduction in the SCF with a reducing agent (i.e., hydrogen and alcohols), thermal reduction in the SCF and thermal decomposition in an inert atmosphere or chemical conversion after depressurization.³⁸ SCFD is convenient for deposition of metallic species having a poor volatility or low thermal stability.^{38,46} Solvent scCO₂ power and sorption of metal complex are adjusted by pressure and temperature change as well as the contact time of SCF solution and the polymeric substrate.

SCFD was mainly considered for production of nanostructured materials for catalysis, electronics and optics.^{38,47} A great potential of the SCFD for fabrication of medical devices has been recognized through the recent reports on scCO₂-aided deposition of metal species with antibacterial activity, namely silver ions onto silicone,⁴⁸ ultra-high molecular-weight-polyethylene films,⁴⁹ and cotton.⁵⁰ Fluorinated metal chelates are well known for excellent solubility in scCO₂.⁴⁶ Zinc bis(2-thenoyltrifluoroacetate), Zn(TTA)₂, which is soluble in scCO₂ at pressures above 15 MPa and temperatures above 65 °C was used as a ZnO precursor for supercritical deposition onto poly(ethylene terephthalate) (PET) films.^{51,52}

ScCO₂ has been recently proven as efficient aid in prefoaming of PLA/clay nanocomposite pellets obtained by melt compounding for dispersing the nanofiller prior to extrusion and injection moulding.²² To the best of our knowledge, there is no report on using scCO₂ as a medium for deposition and foaming agent in a single process for production a three-dimensional polymer/inorganic filler composite. This study was therefore aimed to investigate feasibility of a coupled scCO₂-assisted deposition–foaming process followed by *in situ* synthesis of ZnO for fabrication of porous PLA–ZnO and PLA–PCL–ZnO composite scaffolds for potential use in BTE. The idea was to use scCO₂ both as a physical blowing agent and medium for deposition of organometallic precursors in a single step-process performed at relatively low operating temperature (below PLA melting temperature). Material properties of PLA–ZnO and PLA–PCL–ZnO composite scaffolds relevant for BTE applications were studied to justify applicability of the proposed coupled scCO₂-assisted deposition and foaming process. In this regard, the influence of PCL and deposited mineral filler content on scaffolds' properties was analyzed in detail.

EXPERIMENTAL

Materials

Poly(lactide) (PLA, Ingeo™ Biopolymer 3052D, NatureWorks LLC, Minnetonka, Minnesota, USA), poly(ε-caprolactone) (PCL, $M_n = 80,000$, Aldrich, Missouri, USA) and chloroform (98.3%, Lachema, Neratovice, Czech Republic) were used to prepare polymeric blends by solvent casting method. PCL and PLA solutions (0.067 g/mL) were left in separate glasses overnight. Eight-hour mixing of solutions using a magnetic stirrer at 700 rpm and ambient conditions followed. Thereafter, mixture was poured into a Petri dish to dry in air for ten days (almost a month before experiments). Samples were vacuum dried at 40 °C for 3 h. Homogenous blends in the form of films containing 1, 5, and 10 wt % of PCL denoted as B1, B5, and B10, respectively, were chosen for further tests. Zinc acetate

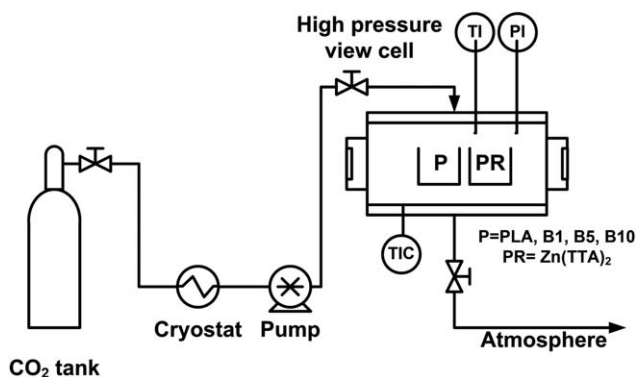


Figure 1. The process for production of polyester composite scaffolds.

dihydrate (Riedel-de-Haën, Germany), 2-thenyltrifluoroacetone (HTTA, 99%, Aldrich, Missouri, USA) and dichloromethane (Lachner, Neratovice, Czech Republic), absolute ethanol (p.a. Merck KgaA, Darmstadt, Germany), and *n*-hexane (VWR, Fontenay-sous-Bois, France) were used to produce metalorganic precursor. Carbon dioxide (99.9%, Messer-Tehnogas AD, Belgrade, Serbia) was used to deposit metalorganic precursor and foam polymeric substrates. Hydrazine hydrate, 80% (hydrazine, 51%) purchased from Acros Organics (New Jersey, USA) was used for conversion of precursor to ZnO after deposition.

Synthesis of the Precursor

The precursor, $\text{Zn}(\text{TТА})_2$, was synthesized as described previously: 1 g (4.56 mmol) of $\text{Zn}(\text{CH}_3\text{COO})_2 \cdot 2\text{H}_2\text{O}$ was solubilized in 20.0 mL of water, and 2.25 g (9.12 mmol) of HTTA was solubilized in 40.0 mL of dichloromethane.^{51,53} The $\text{Zn}(\text{CH}_3\text{COO})_2 \cdot 2\text{H}_2\text{O}$ solution was added into the HTTA solution in the form of drops, forming a white precipitate in a $\text{CH}_2\text{Cl}_2/\text{water}$ mixture. The precipitate was filtered, resolubilized in 50.0 mL of ethanol, and reprecipitated in 100 mL hexane.

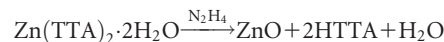
The $\text{Zn}(\text{TТА})_2$ precipitate was dried in an oven at 60°C for 24 h, producing a white powder. The yield was $79.6 \pm 4.3\%$ which is in accordance to the previous report.⁵¹

Production of Composite Scaffolds

Process of SCFD of $\text{Zn}(\text{TТА})_2$ into PLA was performed in a high pressure unit represented schematically by Figure 1. The polymer (P) (0.24 ± 0.04 g) and the precursor (PR) samples (15 mg) were placed in the separate open glass receipts inside the high pressure view cell previously elsewhere.⁵⁴ The cell was filled with CO_2 and pressurized to 30 MPa and 110°C . These conditions were chosen in accordance to previously tested melting behavior of PLA and PCL using DSC under high CO_2 pressure^{43,55} as well as data on solubility of $\text{Zn}(\text{TТА})_2$ in scCO_2 (Supporting Information Figure S1 and available literature data).^{51,52}

The process for production of PLA–ZnO and PLA–PCL–ZnO composite scaffolds involved following steps: (1) SCFD of the precursor into polymer melt, (2) foaming through pressure quench, and (3) *in situ* synthesis of ZnO (Figure 2).

Deposition (impregnation) time was varied from 1 to 15 h aiming to achieve as high as possible impregnation yield of the precursor. In the second step fast depressurization at rate of 5 MPa/s was applied to create a porous structure. Finally, scaffolds impregnated with precursor were treated with hydrazine solution in absolute ethanol for 3 h with reflux. One hundred fifty microliters of 51% hydrazine was dissolved in 20 mL of absolute ethanol. Samples were washed by ethanol and dried under vacuum. The following net chemical reaction occurs in the solution:



Impregnation yield $I^{\text{Zn}(\text{TТА})_2}$ was calculated with respect to the mass of $\text{Zn}(\text{TТА})_2$ dissolved in scCO_2 at given pressure and

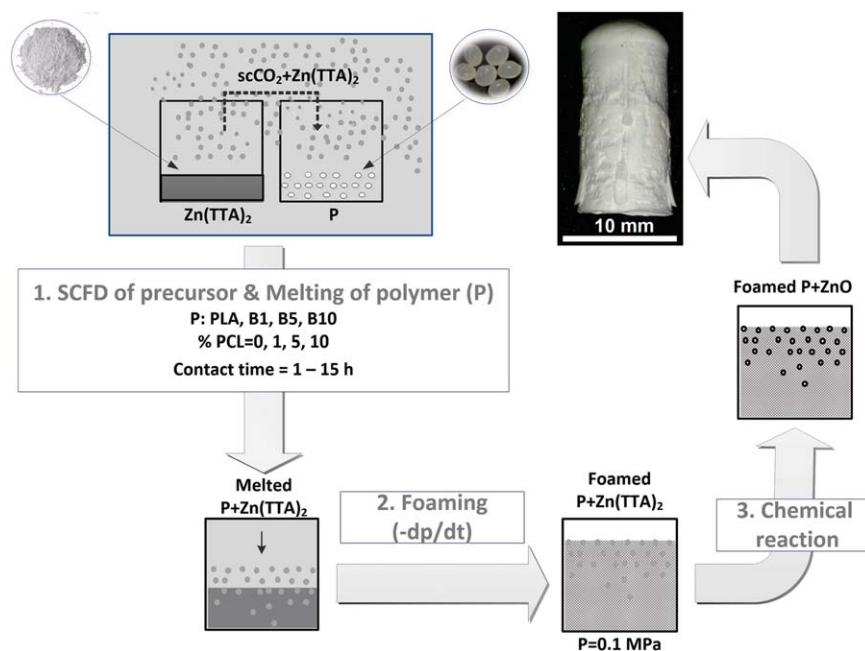


Figure 2. Processing route for production of composite scaffolds. [Color figure can be viewed at wileyonlinelibrary.com]

temperature conditions during given time and cell volume ($m_{\text{Zn(TTA)}_2}^{\text{scCO}_2}$) using eq. (1):

$$I_{\text{Zn(TTA)}_2}^{\text{Zn(TTA)}_2}(\%) = \frac{m_{\text{Zn(TTA)}_2}^{\text{imp.}}}{m_{\text{Zn(TTA)}_2}^{\text{scCO}_2}} \times 100, \quad (1)$$

where $m_{\text{Zn(TTA)}_2}^{\text{imp.}}$ is mass of the precursor impregnated at given pressure and temperature conditions for the given time of impregnation. It is determined gravimetrically as differential mass of the polymeric substrate before and after impregnation. Solubility of Zn(TTA)_2 in scCO_2 was determined by using static method described elsewhere.⁵⁶ The content of ZnO in the composite scaffolds was calculated on the basis of the amount of precursor impregnated into substrates according to the chemical reaction.

Characterization Methods

Fourier-transform infrared (FTIR) spectroscopy was used to analyze synthesized precursor in a BOMEM (Hartmann & Braun) spectrometer. Attenuated total reflection Fourier transform infrared (ATR-FTIR) spectroscopy was used to characterize composites in a Thermo Nicolet Avatar 370 FT-IR with Smart Performer ATR unit using a ZnSe crystal.

Scaffold texture was analyzed by optical microscopy using a digital microscope (VHX-600DSO, Keyence, Japan). Cryofractured samples sputtered with Au were used to study morphology by field emission scanning electron microscope (FESEM, Supra 40, SE2, Carl Zeiss, Germany) operated at an accelerating voltage of 10 kV. The image processing was carried out using ImageJ software, developed by National Institutes of Health, USA, to estimate the average pore diameter.

Helium pycnometer (AccuPyc 1330, Micromeritics Instruments Inc., Norcross, GA) was used to measure the true density of materials. Mercury intrusion porosimetry was used to determine pore size distribution, mean pore diameter (d_{50}), and open porosity of the neat scaffolds using Mercury Porosimeter Pascal 140 and 440 (POROTEC GmbH, Germany). In addition, water displacement method, ASTM D792 was used to investigate densities of the foamed samples containing Zn complex. Upper and lower half of the composite scaffolds were used for the tests to investigate change of porosity and/or d_{50} change along axial direction.

X-ray diffraction (XRD) patterns were taken in reflection mode (Cu $\text{K}\alpha$ radiation) in the 2θ range from 2° to 80° on a Seifert XRD 3003 device (GE Sensing & Inspection Technologies GmbH) with a step size of 0.05° .

Thermogravimetric and differential thermal analysis (TGA/DTA) were performed using a simultaneous thermal analyzer STA 503 (BAEHR Thermo-Analyse GmbH, Germany). TGA tests were conducted to monitor corresponding weight loss in the temperature range of $25\text{--}1000^\circ\text{C}$ under dry N_2 atmosphere (2 L/h). For the degradation kinetic analysis, each sample was heated using a heating rate of $10^\circ\text{C}/\text{min}$ from 25 to 1000°C , following a constant temperature of 1000°C for an hour and cooling down to 25°C using a cooling rate of $10^\circ\text{C}/\text{min}$.

Compression tests were carried out according to the standard test method ASTM C773-88 using a universal testing machine

(Zwick/Roel, Z005, Germany) to study the mechanical stability of the scaffolds. Cylindrical-shaped foam samples had height to diameter ratio of 2 (approximately 15 mm/7.5 mm) and 10 samples were tested per formulation for statistical significance. The monoliths were compressed at a constant speed of 0.5 mm/min, and the force was measured until the monoliths cracked. The force was applied using half-sphere and the preload was 1 N.

Sessile drop method was used to study the wettability of films of neat PLA and its blends which were used for scaffold preparation. Contact Angle System OCA (DataPhysics Instruments GmbH) and software (SCA Ver. 5.0.1.) were used to analyze water and saline contact angle (CA). The CA formed was defined as the angle between the solid/liquid and liquid/vapor interface, respectively. Ten samples from various surface positions were used for the CA measurements to encounter eventual surface heterogeneities. Surface topography and surface roughness of flatten PLA bead and its blend with 10 wt % of PCL (B10) in the form of film were analyzed using a 3D surface profilometer (Optical Imaging Profiler PLu 2300, Sensofar) according to ISO 25178. Confocal objective 20X EPI was used. The analysis of 3D measurements was performed using the software package SensoMap Plus.

RESULTS AND DISCUSSION

Identification of Precursor Synthesis and Its Deposition onto Scaffolds

The complex formation of the precursor Zn(TTA)_2 was confirmed through the FTIR spectrum (Figure 3) that shows peaks at 1601 cm^{-1} (vs), 1580 cm^{-1} (vs), 1540 cm^{-1} (vs) ($\text{C}=\text{O}$) and 1508 (s) ($\text{C}=\text{C}$) that are typical for the β -diketonate ligand.⁵¹ In addition, peaks at 1458 cm^{-1} (s), 1410 cm^{-1} (vs), 1352 cm^{-1} (s), 1303 cm^{-1} (vs), 1255 cm^{-1} (s), 1233 cm^{-1} (s) (thienyl ring); 1190 cm^{-1} (vs) (C-F); 846 cm^{-1} (s), 861 cm^{-1} (s), 933 cm^{-1} (s) (C-H out-plane thienyl); and 790 cm^{-1} (s), 723 cm^{-1} (s) (C-CF_3) testify presence of Zn(TTA)_2 .⁵⁷ The broad band at spectral region of $3300\text{--}3500\text{ cm}^{-1}$ is attributed to water molecules that complete the coordination sphere of Zn^{2+} .

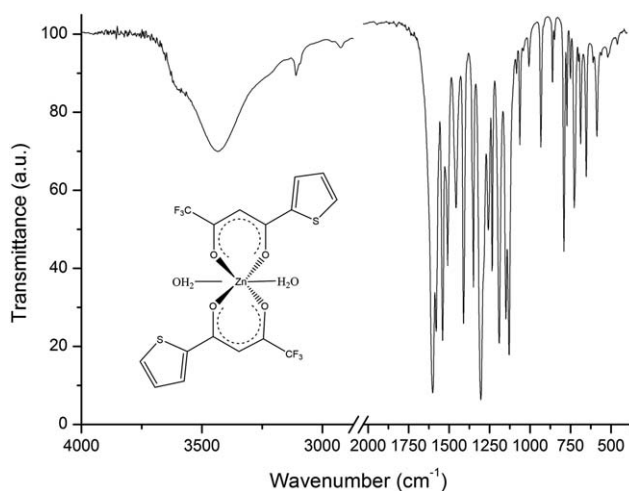


Figure 3. FTIR of prepared precursor: $\text{Zn(TTA)}_2 \cdot 2\text{H}_2\text{O}$.

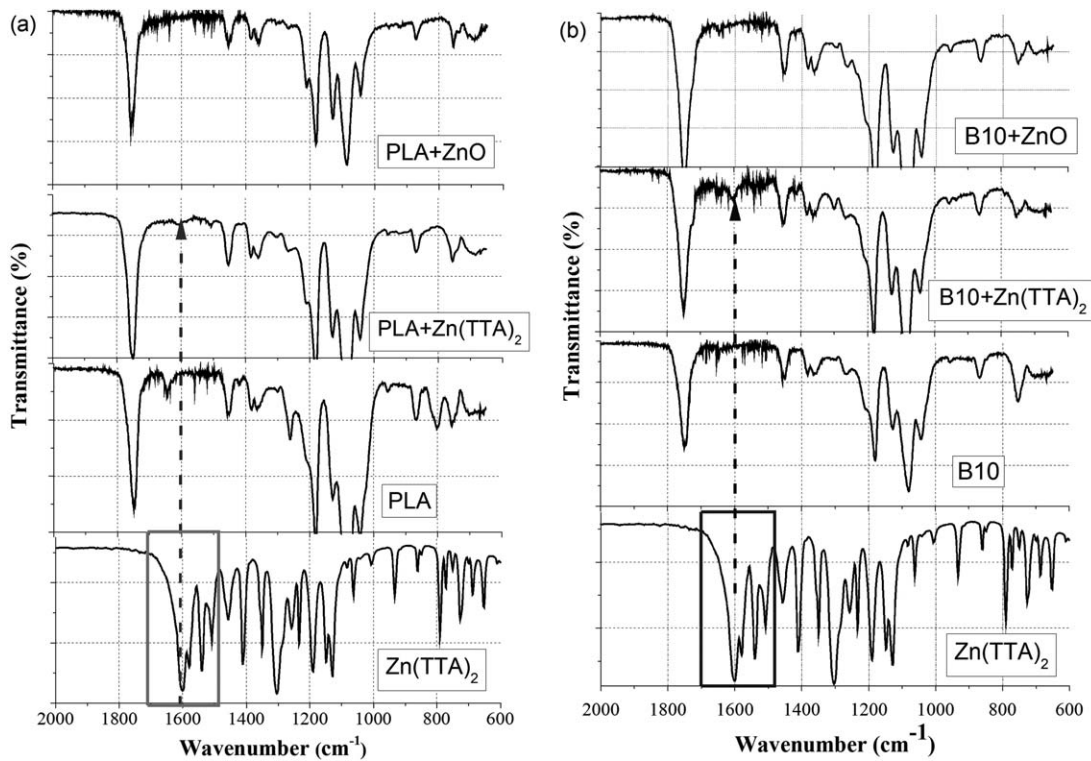


Figure 4. ATR-FTIR spectra of (a) PLA and (b) B10 scaffolds loaded with ZnO and precursor $\text{Zn}(\text{TTA})_2$ compared to nontreated samples (PLA, B10) and pure $\text{Zn}(\text{TTA})_2$.

Comparative analysis of ATR-FTIR spectra of (a) PLA and (b) B10 scaffolds loaded with precursor and ZnO is displayed in Figure 4 where nontreated foam samples and pure precursor serve as reference. Group of the typical β -diketonate ligand peaks at 1601 cm^{-1} (vs), 1580 cm^{-1} (vs), 1540 cm^{-1} (vs) (C=O) and 1508 cm^{-1} (s) (C=C) was observed for both PLA and B10 scaffolds impregnated with the precursor. Increased intensity of these peaks indicated a higher amount of the precursor impregnated into B10 scaffold. In the case of B10- $\text{Zn}(\text{TTA})_2$ the peaks at 1410 cm^{-1} (vs) and 1303 cm^{-1} (vs), (thienyl ring) were also more evident which could be due to a higher amount of deposited precursor. Absence of characteristic peaks of the Zn complex after its conversion to oxide was evidenced for both PLA and B10 scaffolds (Figure 4).

Impregnation yield of the precursor ($I^{\text{Zn}(\text{TTA})_2}$) reported for tested PLA-based substrates and the given SCFD operating pressure and temperature (30 MPa, 110°C) were ranged from 2.4% to 9.3% (Table I). The percentage amount of impregnated precursor with respect to initial mass of the zinc complex ($I^{\text{Zn}(\text{TTA})_{2,0}}$) ranged from 1.4% to 7.5% (Table I). Corresponding ZnO content in the composite scaffolds was ranged from 0.04 to 0.15 mg (0.018–0.045 wt %) (Supporting Information Figure S1). Solubility of $\text{Zn}(\text{TTA})_2$ in scCO_2 at 30 MPa and 110°C ($\rho_{\text{CO}_2} = 628.3\text{ kg/m}^3$) for the contact time of 1–15 h ($6.5\text{--}13.3 \cdot 10^{-4}\text{ kg/kg}$) was one order of magnitude higher (Supporting Information Figure S1a) than previously reported at 20 MPa and 85°C ($\rho_{\text{CO}_2} = 565.7\text{ kg/m}^3$).⁵¹ On the other hand, values of $I^{\text{Zn}(\text{TTA})_{2,0}}$ (Table I) were 4–20 times lower than reported for SCFD of $\text{Zn}(\text{TTA})_2$ onto PET films at 20 MPa and 85°C

($\rho_{\text{CO}_2} = 565.7\text{ kg/m}^3$).⁵¹ This can be explained with an increased affinity of the metal complex to the SCF phase at higher scCO_2 density.

In the case of the neat PLA, the highest impregnation yield of $\text{Zn}(\text{TTA})_2$ (4.84%) was achieved after 2 h (Table I). Longer periods resulted in a decreased quantity of the precursor impregnated into the PLA-based substrates. This phenomenon can be attributed to the increased crystallinity of the polyester substrate over time at high processing temperature above glass transition (T_g) and/or melting temperature (T_m).⁵¹ Along with the swelling of polymer exposed to scCO_2 , an increase of the processing temperature above T_m (for semicrystalline polymers) and exposure period result in an enhanced mobility and a better organization of the polymer chains. Increased crystallinity consequently results in a lower scCO_2 sorption of the precursor by

Table I. Effect of Deposition Time and PCL Content on the Impregnation Yield at 30 MPa and 110°C

Time (h)	PCL (wt %)	$I^{\text{Zn}(\text{TTA})_2}$ (%)	$I^{\text{Zn}(\text{TTA})_{2,0}}$ (%)
1	0	2.43 ± 0.02	1.57 ± 0.01
2	0	4.84 ± 0.02	4.32 ± 0.02
3	0	3.13 ± 0.03	2.93 ± 0.02
5	0	1.72 ± 0.01	1.73 ± 0.01
15	0	1.47 ± 0.01	1.44 ± 0.01
2	1	7.80 ± 0.04	6.13 ± 0.03
2	10	9.30 ± 0.04	7.48 ± 0.03

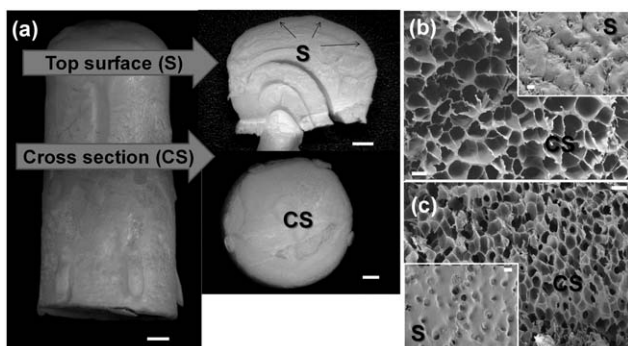


Figure 5. (a) Digital image of top surface (S) and cross section (CS) of the representative nanocomposite scaffold (B10-ZnO) (scale bar = 1 mm), and SEM images of S and CS of (b) PLA-ZnO and (c) B10-ZnO composite scaffolds (scale bars = 20 μm).

the polymer bulk. Positive effect of blending PLA with PCL on impregnation of the precursor into substrate could be due to plasticizing effect of the PCL.⁵⁸ Lower percentage of PCL (up to 10%) was added to avoid phase separation due to immiscibility of these two polymers.⁵⁸

Structural Properties

Optical microscopy and SEM were used to evaluate scaffolds' morphology. Digital images of a representative composite scaffold, B10-ZnO, as well as SEM analysis revealed formation of the layers at the very top of the foam cylinder (Figure 5). This was due to the absence of the confinement (sealer of the Teflon mold used for foaming) which led to a faster cell growth during CO₂ escape from the polymer phase, their merging and finally collapsing during decompression step (Figure 2). The cross-sectional SEM images [Figure 5(b,c)] show porous inner structure of the PLA-ZnO and B10-ZnO foams having micron-sized pores ($d_{50} = 26.2 \pm 6.7 \mu\text{m}$ and $d_{50} = 16.7 \pm 3.9 \mu\text{m}$, respectively).

Mercury intrusion porosimetry was used to test pore size distribution and open porosity of the upper and lower half of the neat scaffolds. Monomodal pore size distribution was observed for all the samples. The results of the porosimetry tests (Figure 6 and Supporting Information Table S1) present mean values obtained by testing an upper and lower half of the scaffolds. Determined open porosity of the neat PLA, B1, B5, and B10 scaffolds was 77, 69.8, 68.7%, and 72% (Supporting Information Table S1 and Figure 6). These values fall in the range of reported porosity of the trabecular bone (50–90%) which allows nutrient diffusion and exposure to circulating growth factors.⁵⁹ Mean pore diameter of the neat scaffolds determined by porosimetry was in the range of 2.9–5.6 μm (Supporting Information Table S1). Decrease of open porosity and average pore diameter of the scaffolds of blends (Figure 6 and Supporting Information Table S1) could be due to a faster crystallization of PLA in presence of PCL^{14,15} which constrains pore growth during decompression step (Figure 2). Increase of PCL content from 1 to 10 wt % results in slight increase of open porosity and average pore diameter (Figure 6 and Supporting Information Table S1) which could be due to a more pronounced effect of PLA and PCL immiscibility^{16,60} and less order in arranging of polymer

chains. Values of d_{50} determined by Hg intrusion porosimetry are 4–5 times smaller compared to those observed by SEM analysis of PLA-ZnO and B10-ZnO (16.7–26.2 μm) (Supporting Information Table S1). One reason for the underestimation of pore size by using Hg intrusion porosimetry can be due to assumption of cylindrical pores in Washburn equation.⁶¹ On the other side, inner large pores connected with outer small pores are detected only at high pressures and therefore counted as small pores.⁶² Mercury intrusion measurements were therefore complemented with SEM image analysis to get quantitative information on pore size and distribution (Supporting Information Table S1 and Supporting Information Figure S2). Although SEM images provide direct and reliable data they refer to a limited area of a specific cross section. SEM images were recently used to analyze pore size and porosity of PLA and PLA-ZnO scaffolds.^{26,63} Similar porosity (81%) was reported for the neat PLA foamed using scCO₂ at the same pressure and somewhat higher temperature (131 °C), whereas pore size varied between several micrometers and a few millimetres.²⁶ Nondegraded PLA and PLA-ZnO (1 wt % of ZnO) scaffolds obtained using solvent casting/particulate leaching method in the study of Lizundia *et al.*⁶³ showed uniformly distributed pores of about 187 ± 54 and $184 \pm 37 \mu\text{m}$ for 50% and 90% porous scaffolds respectively.

After precursor deposition, change of d_{50} values in the axial direction was shown to be negligible except in the case of B10

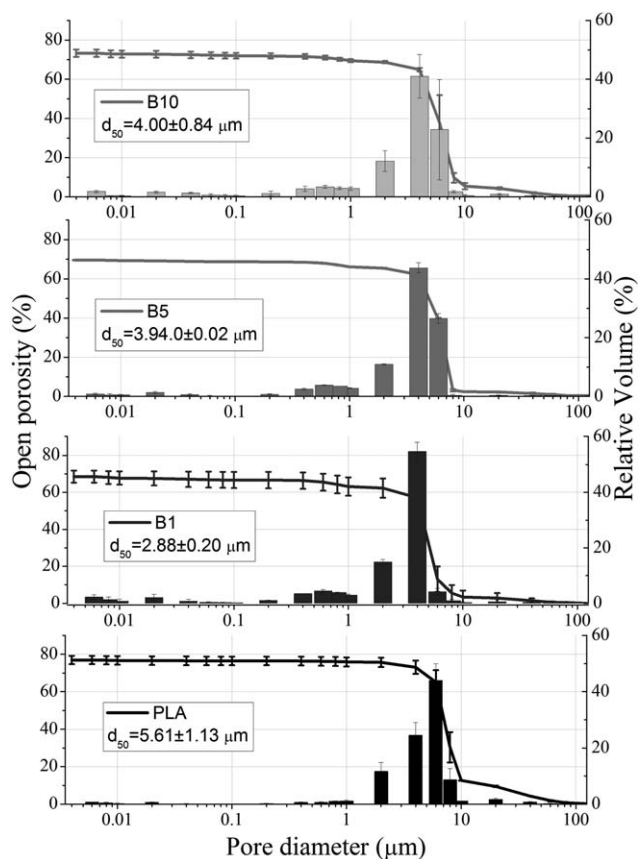


Figure 6. Influence of PCL content in PLA scaffolds on pore size distribution and open porosity.

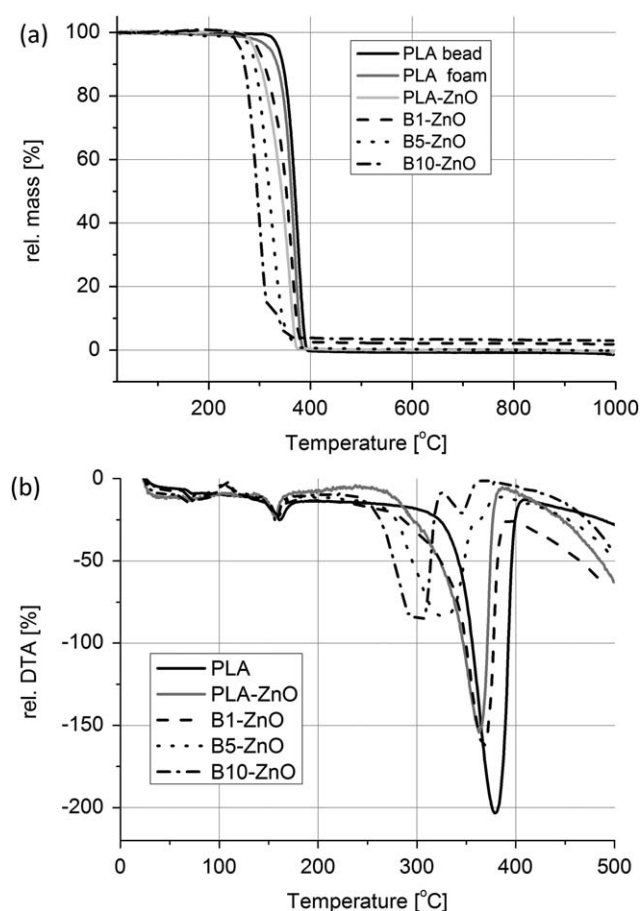


Figure 7. (a) Influence of %PCL on plasticization and crystallization of PLA-ZnO composites and (b) kinetics of thermal decomposition of PLA-ZnO composites.

scaffold (Supporting Information Figure S2a). Observed variations of d_{50} in axial direction for the tested scaffolds had no significant effect on the open porosity decrease (0.2–6.5%). Change of porosity along axial direction of scaffolds containing precursor was negligible except in the case of B10-PR (Supporting Information Figure S2c). Opposite to the neat B10 scaffold (Supporting Information Figure S2b), the porosity of scaffold containing Zn complex (B10-PR) increases toward top (Supporting Information Figure S2c). This could be due to a higher concentration of the precursor particles in the upper part of the scaffold and their positive effect on bubble nucleation and foaming ability.³⁰

Pore size and pore interconnectivity has considerable biological importance for bony ingrowths. Minimum pore size of 30–100 μm is required for cell migration, vascularization and transportation processes.⁶⁴ Pores having a diameter greater than 50 μm are reported for positive impact on osteogenic outcomes while pores with diameter greater than 10 μm contribute to a higher bone inducing protein adsorption, ion exchange and bone-like apatite formation.⁵⁹ PLA membranes with the pore diameter of 10–20 μm were proved for the highest efficiency in guided bone tissue regeneration.¹¹ This *in vivo* study showed no significant effect of pore size (10–200 μm) of PLA membrane on efficiency

in treatment of diaphyseal defect in female rabbits ($\phi 10$ mm) within six months.¹¹ Recent *in vitro* tests of the osteoblast-like MG-63 cell line performed on the porous PCL and PLA/PCL membranes (with pore diameters up to 30 μm) confirmed both biocompatibility and demonstrated that cells adhered well to the material surface of both types of membranes.¹²

Thermal Properties

Namely, PLA and PCL form a partially miscible blend, whereby an amount of amorphous PCL is dissolved in the PLA-rich phase leading to a depression of the glass and melting temperature shift to lower values.¹⁶ Reportedly, PCL serves as a nucleating agent to promote PLA crystallization when blended with PLA.^{16,60} The shift of onset and offset decomposition temperatures of PLA-ZnO in comparison to the neat PLA film and foam (19 and 10 °C, respectively) indicated an effect of ZnO on thermal stability (Figure 7). Alkali earth metal oxide including ZnO fillers are proven to catalyze degradation of the polyesters including PLA especially at high processing temperatures (i.e., during melt-processing).^{63,65} DTA curves of B5-ZnO and B10-ZnO composite scaffolds show a shift of decomposition peaks to the lower temperatures in comparison to PLA-ZnO and B1-ZnO (Figure 7b). Appearance of two decomposition peaks observed for the composite scaffolds obtained from blends with 5 and 10 wt % of PCL (B5-ZnO and B10-ZnO) indicates a more pronounced effect of PLA and PCL immiscibility.

A shift of glass transition and melting temperature peak to the lower values observed for the ZnO composites obtained from blends of PLA with PCL (B1, B5, and B10) confirmed plasticizing effect of PCL (Figure 7b). Accordingly, the appearance of cold crystallization peak of ZnO-composites of the blends in comparison to PLA-ZnO indicated positive effect of 1–10% PCL on crystallization rate of PLA in presence of scCO_2 .

Composites scaffolds with higher amount of PCL, B5-ZnO, and B10-ZnO had the fastest decomposition rate (Table II). However, similar rate of thermal decomposition of PLA foam and PLA-ZnO scaffold (Table II) evidenced that effect of ZnO at the level reported in the study (0.018–0.045%) and blending of PLA with 1–10% of PCL decrease thermal stability at acceptable level when exposed to scCO_2 at given pressure and temperature conditions (30 MPa, 110 °C, 2 h).

Table II. Kinetics of Thermal Decomposition

Sample	Decomposition temperature (°C)	% wt/min
PLA bead	371	-21.5
PLA foam	363	-22.2
PLA-Zn(TTA) ₂	364	-22.3
PLA-ZnO	352	-22.8
B10 film	367	-19.0
B10 foam	363	-19.8
B10-ZnO	292	-19.3
B5-ZnO	320	-17.6
B1-ZnO	357	-17.6

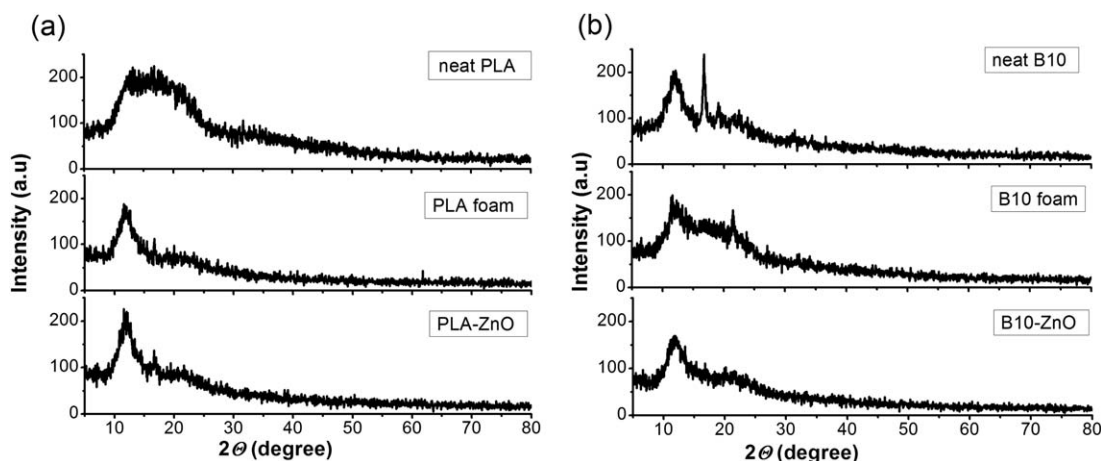


Figure 8. Representative X-ray diffraction patterns of (a) PLA and (b) B10 samples.

According to the recent report, a significant effect of ZnO on the thermal stability of PLA composite scaffolds is expected at higher contents of the filler (≥ 1 wt %).⁶³

XRD Analysis

The influence of blending of PLA with PCL, $scCO_2$ foaming and deposited ZnO on crystalline structure was studied by XRD. Comparative XRD analysis patterns of the untreated PLA and B10 samples are shown in Figure 8. A broad and intense peak between 12° and 22° in the XRD diffractogram of the non-treated PLA (Figure 8a) indicates mainly amorphous structure with presence of either small or imperfect crystallites.⁶⁶ Blending of PLA with 10% of PCL resulted in appearance of crystalline peaks at $2\theta = 12^\circ$, 16.7° , 19.2° , and 21.7° (Figure 8b). The sharp and intense peak at $2\theta = 16.7^\circ$ is ascribed to α form of PLA crystallized in a pseudo-orthorhombic unit cell which contains two 10_3 helices. This peak can be also observed in diffractograms of foamed PLA and also PLA-ZnO composite. In the latter case its intensity is increased. The peak at 16.7° broadening is observed for the neat B10 scaffold. With ZnO deposition onto B10 scaffold the peak sharpens. For both PLA and B10 deposition of ZnO seems to have positive effect on formation of α crystallites. Diffractions at $2\theta = 12^\circ$, 19.2° , and 21.8° are associated with PLA crystallization in a triclinic unit cell, in which L-lactide and D-lactide segments are packed parallel taking a 3_1 helical conformation.^{67,68} Peak at $2\theta = 12^\circ$ is the most intensive crystalline peak observed in the diffractograms of the tested scaffolds.

Coupling addition of 10% of PCL and $scCO_2$ treatment resulted in disappearance of peak at 16.7° and appearance of peak at 22° . XRD patterns of the both PLA-ZnO and B10-ZnO composite scaffolds, however, displayed an intensive peak at 12° and a broad peak at 22° . Accordingly, both CO_2 treatment and ZnO deposition affect crystalline structure reorganization. It was previously shown that both method of ZnO incorporation and its content inside the matrix can affect crystalline structure of the final PLA-ZnO composite material.^{37,69} Presence of small amount of ZnO incorporated by melt blending ($\leq 0.5\%$) was proven to have positive influence on crystallinity, whereas

higher loadings (1–3%) result in slightly crystalline to completely amorphous structure.⁶⁹ Previously reported XRD pattern of PLGA/ZnO (0.55%) nanocomposite particles synthesized by physicochemical solvent/nonsolvent method showed no crystalline peaks.³⁷ The SCFD of the Zn precursor and its posterior transformation to ZnO therefore seemed to provide a good dispersion of the filler and its interaction with the matrix.

Reportedly, XRD patterns of ZnO phase obtained from the $Zn(TTA)_2$ exhibit characteristic peaks at 2θ of 31.90° , 34.55° , 36.40° , 47.75° , and 56.75° which are associated with the reflections of 100, 002, 101, 102, and 110 planes.⁵³ These peaks except $2\theta = 31.9^\circ$ and $2\theta = 36.4^\circ$ ascribed respectively to the diffraction planes of (100) and (101) are hard to designate due to a very low filler loading ($\leq 0.5\%$).⁶⁹ However, XRD patterns of neat and ZnO containing scaffolds, in particular in the case of B10, are evidently different. In the case of PLA-ZnO, an increased intensity of the peaks at 12° and 16.7° and appearance of peak at 22° is observed. A broad diffraction peak observed for B10 foamed with $scCO_2$ is not visible on the XRD pattern of its composite which indicates increased crystalline regularity thereof.

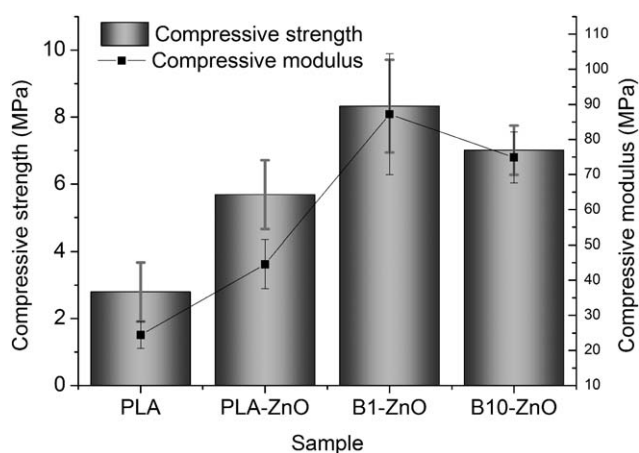


Figure 9. Influence of ZnO and %PCL in PLA on compressive strength and modulus.

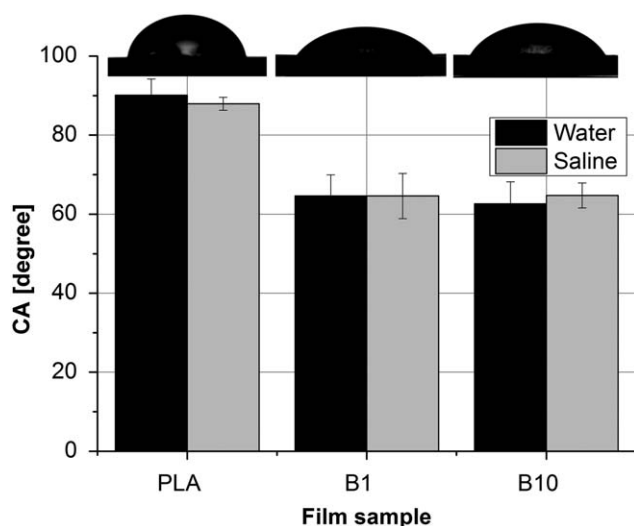


Figure 10. Effect of PCL content on wettability of PLA films.

Mechanical Properties

Mechanical properties of the scaffold need to match those of the tissues at the site of implantation. Compressive strength and moduli of bone tissue depends on species and anatomical site. Reported values for compressive strength and moduli for the human cancellous bone are in the range of 2–12 and 20–500 MPa, respectively. Values of compressive strength and moduli of the compact bone are 130–230 and 7000–30,000 MPa, respectively.⁷⁰ Compressive strength of PLA–ZnO and PLA–PCL–ZnO composite scaffolds in this study ranged from 2.8 to 8.3 MPa while corresponding compressive moduli were in the range of 24.4–87.2 MPa (Figure 9). These values of compressive strength and moduli correspond to the ones reported for the trabecular bone.

PLA–ZnO composite scaffold obtained after 2 h impregnation of precursor (%ZnO = 0.037%) had a two times higher compressive (5.68 MPa) strength in comparison to neat PLA scaffold (2.8 MPa) which was foamed at same decompression rate and after same time of exposure to scCO₂ (2 h). This in accordance to XRD analysis which showed a positive effect of deposited ZnO on crystalline structure of both PLA and B10 scaffolds (Figure 8).

Improved compressive strength of composite scaffolds with 1% and 10% of PCL compared to PLA–ZnO could be due to faster crystallization of PLA in presence of PCL (Figure 9). Accordingly, deformation at maximal force for PLA samples was shown to be $18.5 \pm 0.4\%$ and of blends two times less, $10.5 \pm 0.5\%$.

Somewhat lower value of compressive strength of B10–ZnO could be due to a slower crystallization of the polymer matrix in presence of higher PCL percentage (10 wt %). This indicated that blending of higher PCL amount with PLA due to their partial miscibility could lead to nonuniformity in crystals arrangement and uneven pore distribution. This observation is in accordance with observed increase in open porosity for B10 scaffold (Supporting Information Table S1). Since mechanical strength of a scaffold decreases with porosity, it should be

balanced with the mechanical requirements for the particular tissue that is to be replaced.^{71,72}

Effect of PCL Content in the PLA Films on Wettability

Hydrophilicity is one of the most important materials feature in cell-related studies.⁷³ This is due to the tendency of wettable or hydrophilic surfaces to interact with biological entities or dissolved biomolecules in water. Wettability and surface topography of neat PLA and blends with 1 and 10 wt % PCL were analyzed due to relevance for cell attachment and proliferation. Wettability of the PLA and blends' films was determined by the measurement of the material surface CA. Contact angle is a phase interface property that can be measured directly and it characterizes the drop shape on the solid surface. The influence of PCL content in the PLA films on the water and saline CA change is presented in Figure 10. Accordingly, PLA film changed from the transition region hydrophobic/hydrophilic (CA = 90°) to hydrophilic (CA = 62–64°) when blended with 1–10 wt % of PCL. Similar water CAs were observed for saline on both neat PLA and blends. It can be related with improved crystallization of PLA films in presence of PCL (Figure 8b) which results in surface roughness on nanometer scale and consequently improved hydrophilicity.⁷³

The wettability depends on both chemical composition and surface roughness.⁷³ The value of arithmetical mean surface roughness (Sa) of PLA film was 0.4 μm and it triples after blending with 10% of PCL (1.2 μm) (Supporting Information Figure S2). Heterogeneity and discontinuities of the PLA film surface increased with percentage of added PCL. The optimal value of water CA for various cell adhesion was reported to be in the range of 50–70°.^{73,74} Reportedly, improved roughness positively affects cell adhesion onto PLA materials.^{75,76}

CONCLUSIONS

The processing route involving a subsequent scCO₂-aided deposition and foaming process followed by *in situ* synthesis of ZnO was used for the first time to fabricate biopolyester–ZnO composite scaffolds in a controlled manner. Optimal deposition pressure, temperature and time were set according to PLA thermal behavior under high scCO₂ pressures, solubility of the precursor in the SCF and its deposition yield. Scaffolds of neat PLA and blended with 1–10% PCL showed high open porosity (69–77%) and values of compressive strength of 2.8–8.3 MPa that correspond to trabecular bone. Incorporated amount of ZnO (~0.04 wt %) positively affected compressive strength and had no significant effect on thermal stability of the final foamed product. Utilization of PLA blended with low percentage of PCL (1–10%) was suggested for improved processability of material and compressive strength of the obtained scaffolds. XRD analysis showed that applied procedure for fabrication of PLA-based composite scaffolds provides a good interaction of both scCO₂ and ZnO with polymer substrate and the positive effect on rearrangements of the crystalline structure. Blending of PLA and PCL also improved material wettability and surface roughness which is a relevant factor for cell adherence and proliferation. Analysis of structural, thermal and mechanical properties of biopolyester–ZnO scaffolds testified great potential of

approach for fabrication and/or functionalization of polymeric platforms for bone regeneration. The proposed straightforward processing route for fabrication of metal oxide-polymer composite scaffolds is environmentally friendly, fast, easy to control and suitable for processing thermosensitive polymers. Given a good solubility of a wide range of precursors (β -ketonates, fluorinated β -ketonates, and organometallic complexes) in scCO_2 the presented platform is highly promising for design of novel cellular systems with tunable properties for tissue engineering applications.

ACKNOWLEDGMENTS

Financial support of this work from the Ministry of Education, Science and Technological Development of the Republic of Serbia (project no. III 45017) and DAAD Funding Program Research Stays for University Academics and Scientists (ID 57210259) is gratefully acknowledged.

REFERENCES

1. Feldman, D. *J. Macromol. Sci. Part A* **2016**, *53*, 55.
2. Liao, X.; Zhang, H.; He, T. *J. Nanomater.* **2012**, *2012*, Article ID 836394,
3. Okamoto, M.; John, B. *Prog. Polym. Sci.* **2013**, *38*, 1487.
4. Bergstöröm, J. S.; Hayman, D. *Ann. Biomed. Eng.* **2016**, *44*, 330.
5. Savioli Lopes, M.; Jardini, A. L.; Maciel Filho, R. *Proc. Eng.* **2012**, *42*, 1402.
6. Rajendran, T.; Venugopalan, S. *J. Pharm. Sci. Res.* **2015**, *7*, 960.
7. Salerno, A.; Fernández-Gutiérrez, M.; San Román del Barrio, J.; Domingo, C. *J. Supercrit. Fluids* **2015**, *97*, 238.
8. Meinig, R. P. *Orthop. Clin. North Am.* **2010**, *41*, 39.
9. Dimitriou, R.; Mataliotakis, G. I.; Calori, G.; Giannoudis, P. V. *BMC Med.* **2012**, *10*, 81.
10. Xu, Q.; Pang, M.; Peng, Q.; Jiang, Y.; Li, J.; Wang, H.; Zhu, M. *J. Appl. Polym. Sci.* **2005**, *98*, 831.
11. Pineda, L. M. Meijg, M. B. R. P. *J. Biomed. Mater. Res.* **1996**, *31*, 385.
12. Domalik-Pyzik, P.; Morawska-ChochChochół, A.; Chłopek, J.; Rajzer, I.; Wrona, A.; Menaszek, E.; Ambroziak, M. *E-Polymers* **2016**, *16*, 351.
13. Murariu, M.; Dubois, P. *Adv. Drug Deliv. Rev.* **2016**, *107*, 17.
14. Wu, D.; Zhang, Y.; Yuan, L.; Zhang, M.; Zhou, W. *J. Polym. Sci., Part B: Polym. Phys.* **2010**, *48*, 756.
15. Goriparthi, B. K.; Suman, K. N. S.; Nalluri, M. R. *Polym. Compos.* **2012**, *33*, 237.
16. Yeh, J.; Wu, C.; Tsou, C.; Chai, W.; Chow, J.; Huang, C.; Chen, K.; Wu, C.; Yeh, J.; Wu, C.; Tsou, C.; Chai, W. *Polym. Plast. Technol. Eng.* **2009**, *48*, 571.
17. Okan, B. S.; Marset, A.; Seyyed Monfared Zanjani, J.; Sut, P. A.; Sen, O.; Çulha, M.; Menciloglu, Y. *J. Appl. Polym. Sci.* **2016**, *133*, DOI: 10.1002/app.43490.
18. Kothapalli, C. R.; Shaw, M. T.; Wei, M. *Acta Biomater.* **2005**, *1*, 653.
19. Mosanenzadeh, S. G.; Naguib, H. E.; Park, C. B.; Atalla, N. *J. Appl. Polym. Sci.* **2014**, *131*, DOI: 10.1002/app.39518.
20. Llorens, E.; del Valle, L. J.; Puiggali, J. *Macromol. Res.* **2015**, *23*, 636.
21. Serra, T.; Mateos-Timoneda, M. A.; Planell, J. A.; Navarro, M. *Organogenesis* **2013**, *9*, 239.
22. Zhao, H.; Zhao, G.; Turng, L.-S.; Peng, X. *Ind. Eng. Chem. Res.* **2015**, *54*, 7122.
23. Chávez-Montes, W.; González-Sánchez, G.; Flores-Gallardo, S. *Polymers* **2016**, *8*, 154.
24. Yang, Q.; Zhang, G.; Ma, Z.; Li, J.; Fan, X. *J. Appl. Polym. Sci.* **2015**, *132*, DOI: 10.1002/app.42576.
25. Karimi, M.; Heuchel, M.; Weigel, T.; Schossig, M.; Hofmann, D.; Lendlein, A. *J. Supercrit. Fluids* **2012**, *61*, 175.
26. Frerich, S. C. *J. Supercrit. Fluids* **2015**, *96*, 349.
27. Kiran, E. *J. Supercrit. Fluids* **2016**, *110*, 126.
28. Kiran, E. *J. Supercrit. Fluids* **2010**, *54*, 308.
29. Armentano, I.; Dottori, M.; Fortunati, E.; Mattioli, S.; Kenny, J. M. *Polym. Degrad. Stab.* **2010**, *95*, 2126.
30. Keshtkar, M.; Nofar, M.; Park, C. B.; Carreau, P. *J. Polym.* **2014**, *55*, 4077.
31. Nofar, M.; Tabatabaei, A.; Park, C. B. *Polymer* **2013**, *54*, 2382.
32. Parham, S.; Wicaksono, D. H. B.; Bagherbaigi, S.; Lee, L.; Nur, H. *J. Chin. Chem. Soc.* **2016**, *63*, 385.
33. Ansari, M. A.; Khan, H. M.; Khan, A. A.; Sultan, A.; Azam, A. *World J. Microbiol. Biotechnol.* **2012**, *28*, 1605.
34. Fielding, G. A.; Smoot, W.; Bose, S. *J. Biomed. Mater. Res. A* **2014**, *102*, 2417.
35. Feng, P.; Wei, P.; Shuai, C.; Peng, S. *PLoS One* **2014**, *9*, e87755.
36. Memarzadeh, K.; Sharili, A. S.; Huang, J.; Rawlinson, S. C. F.; Allaker, R. P. *J. Biomed. Mater. Res. A* **2015**, *103*, 981.
37. Stankovic, A.; Sezen, M.; Marina, M.; Kaišarevic, S.; Andric, N.; Stevanovic, M. *J. Nanomaterials* **2016**, *2016*, Article ID 9425289.
38. Bozba, S. E.; Erkey, C. *J. Supercrit. Fluids* **2015**, *96*, 298.
39. Kikic, I. *J. Supercrit. Fluids* **2009**, *47*, 458.
40. Shieh, Y. T.; Su, J. H.; Manivannan, G.; Lee, P. H. C.; Sawan, S. P.; Spall, W. D. *J. Appl. Polym. Sci.* **1996**, *59*, 695.
41. Aionicesei, E.; Škerget, M.; Knez, Ž. *J. Supercrit. Fluids* **2008**, *47*, 296.
42. Fujiwara, T.; Yamaoka, T.; Kimura, Y.; Wynne, K. *J. Biomacromol.* **2005**, *6*, 2370.
43. Kuska, R.; Milovanovic, S.; Janowski, J.; Frerich, S.; Zizovic, I.; Ivanovic, J. Presented at the 15th European Meeting on Supercritical Fluids (EMSF), Essen, Germany, May 8–13, **2016**.
44. Chauvet, M.; Saucéau, M.; Baillon, F.; Fages, J. *J. Appl. Polym. Sci.* **2017**, *134*, DOI: 10.1002/app.45067.
45. Kikic, I.; Vecchione, F. *Curr. Opin. Solid State Mater. Sci.* **2003**, *7*, 399.
46. Darr, J. A.; Poliakov, M. *Chem. Rev.* **1999**, *99*, 495.

47. Belmas, M.; Tabata, I.; Hisada, K.; Hori, T. *J. Appl. Polym. Sci.* **2011**, *119*, 2283.
48. Furno, F.; Morley, K. S.; Wong, B.; Sharp, B. L.; Arnold, P. L.; Howdle, S. M.; Bayston, R.; Brown, P. D.; Winship, P. D.; Reid, H. J. *J. Antimicrob. Chemother.* **2004**, *54*, 1019.
49. Morley, K. S.; Webb, P. B.; Tokareva, N. V.; Krasnov, A. P.; Popov, V. K.; Zhang, J.; Roberts, C. J.; Howdle, S. M. *Eur. Polym. J.* **2007**, *43*, 307.
50. Gittard, S. D.; Hojo, D.; Hyde, G. K.; Scarel, G.; Narayan, R. J.; Parsons, G. N. *J. Mater. Eng. Perform.* **2010**, *19*, 368.
51. Mauricio, M. R.; Manso, F. C. G.; Kunita, M. H.; Velasco, D. S.; Bento, A. C.; Muniz, E. C.; de Carvalho, G. M.; Rubira, A. F. *Compos. Part A: Appl. Sci. Manuf.* **2011**, *42*, 757.
52. Maurício, M. R.; Manso, F. C. G.; Kunita, M. H.; Velasco, D. S.; Favareto, A. C. B.; Filho, L. C.; de Carvalho, G. M.; Rubira, A. Presented at the 10th Congresso Brasileiro de Polímeros, Foz do Iguaçu, **2009**.
53. Malandrino, G.; Blandino, M.; Perdicaro, L. M. S.; Fragalà, I. L.; Rossi, P.; Dapporto, P. *Inorg. Chem.* **2005**, *44*, 9684.
54. Milovanovic, S.; Jankovic-Castvan, I.; Ivanovic, J.; Zizovic, I. *Starch Stärke* **2015**, *67*, 174.
55. Ivanovic, J.; Knauer, S.; Fanovich, A.; Milovanovic, S.; Stamenic, M.; Jaeger, P.; Zizovic, I.; Eggers, R. *J. Supercrit. Fluids* **2016**, *107*, 486.
56. Milovanovic, S.; Stamenic, M.; Markovic, D.; Radetic, M.; Zizovic, I. *J. Supercrit. Fluids* **2013**, *84*, 173.
57. Al-Anber, M. A. *Orient. J. Chem.* **2013**, *29*, 1437.
58. Semba, T.; Kitagawa, K.; Ishiaku, U. S.; Hamada, H. *J. Appl. Polym. Sci.* **2006**, *101*, 1816.
59. Karageorgiou, V.; Kaplan, D. *Biomaterials* **2005**, *26*, 5474.
60. Luyt, A. S.; Gasmi, S. *J. Mater. Sci.* **2016**, *51*, 4670.
61. Giesche, H. *Part. Part. Syst. Character.* **2006**, *23*, 9.
62. Scaffaro, R.; Lo Re, G.; Rigogliuso, S.; Ghersi, G. *Sci. Technol. Adv. Mater.* **2012**, *13*, 45003.
63. Lizundia, E.; Mateos, P.; Vilas, J. L. *Mater. Sci. Eng. C* **2017**, *75*, 714.
64. Sakai, R.; John, B.; Okamoto, M.; Seppälä, J. V.; Vaithilingam, J.; Hussein, H.; Goodridge, R. *Macromol. Mater. Eng.* **2013**, *298*, 45.
65. Murariu, M.; Doumbia, A.; Bonnaud, L.; Dechief, A.-L.; Paint, Y.; Ferreira, M.; Campagne, C.; Devaux, E.; Dubois, P. *Biomacromolecules* **2011**, *12*, 1762.
66. Marubayashi, H.; Akaishi, S.; Akasaka, S.; Asai, S.; Sumita, M. *Macromolecules* **2008**, *41*, 9192.
67. Spasova, M.; Manolova, N.; Paneva, D.; Mincheva, R.; Dubois, P.; Rashkov, I.; Maximova, V.; Danchev, D. *Biomacromolecules* **2010**, *11*, 151.
68. Tsuji, H.; Nakano, M.; Hashimoto, M.; Takashima, K.; Katsura, S.; Mizuno, A. *Biomacromolecules* **2006**, *7*, 3316.
69. Pantani, R.; Gorrasi, G.; Murariu, M.; Dubois, P. *Macromol. Mater. Eng.* **2014**, *299*, 104.
70. Velasco, M. A.; Narváez-Tovar, C. A.; Garzón-Alvarado, D. A. *Biomed. Res. Int.* **2015**, *2015*, Article ID 729076.
71. Polo-Corrales, L.; Latorre-Esteves, M.; Ramirez-Vick, J. E. *J. Nanosci. Nanotechnol.* **2014**, *14*, 15.
72. Patel, P. S. D.; Shepherd, D. E. T.; Hukins, D. W. L. *BMC Musculoskelet. Disord.* **2008**, *9*, 137.
73. Slepickova Kasalkova, N.; Slepicka, P.; Kolska, Z.; Svorcik, V. In *Wetting and Wettability*; Aliofkhaezrai, M., Ed.; InTech: Rijeka, Croatia, **2015**; Chapter 12, pp. 324.
74. Tamada, Y.; Ikada, Y. *J. Biomed. Mater. Res.* **1994**, *28*, 783.
75. Navarro, M.; Engel, E.; Planell, J. A.; Amaral, I.; Barbosa, M.; Ginebra, M. P. *J. Biomed. Mater. Res. A* **2008**, *85*, 477.
76. Washburn, N. R.; Yamada, K. M.; Simon, C. G.; Kennedy, S. B.; Amis, E. *J. Biomater.* **2004**, *25*, 1215.